VIP O_2 Reduction

DOI: 10.1002/anie.200800073

A General Approach to the Size- and Shape-Controlled Synthesis of Platinum Nanoparticles and Their Catalytic Reduction of Oxygen**

*Chao Wang, Hideo Daimon, Taigo Onodera, Tetsunori Koda, and Shouheng Sun**

The synthesis of platinum nanoparticles (Pt NPs) with controlled sizes and shapes is an attractive goal in developing highly active platinum catalysts for the synthesis of fine chemicals.[1] Well-dispersed Pt NPs are also an important catalyst for fuel-cell reactions: in commonly studied polymer electrolyte membrane fuel cells (PEMFCs), they catalyze hydrogen oxidation at the anode and oxygen reduction at the cathode.[2] In the oxygen reduction reaction (ORR), the surface of the platinum catalyst tends to be shielded by the electrolyte or a hydroxy layer.[3] As a result, the active sites on the platinum surface are reduced in number, and the efficiency of the catalyst is limited. To improve the ORR activity, platinum catalysts should be either alloyed with various transition metals,[4] or made with controlled shapes to reduce the binding strength between platinum atoms and the adsorbed species. Previous research has revealed that, in a H_2SO_4 medium commonly used for PEMFCs, the ORR activity on Pt(100) is higher than that on Pt(111) owing to the different adsorption rate of sulfates on these facets.[5] Although various methods have been developed to make Pt NPs,[6] controlled synthesis of Pt NPs with a narrow shape distribution has been rarely reported.[7]

We recently reported that monodisperse platinum nanocubes could be made by reduction of platinum acetylacetonate, $Pt(acac)_2$, in the presence of oleic acid, oleylamine, and a trace amount of iron pentacarbonyl, $Fe(CO)_5$.[8] Further synthesis revealed that, by controlling the reaction temperature, monodisperse Pt NPs were readily produced as polyhedrons, truncated cubes, or cubes. This work allowed detailed studies in shape-dependent catalysis for the ORR and for verification of a recent observation that fuel-cell activity of the Pt NP catalyst is independent of the size of the catalyst.[9] Herein we report a general route to monodisperse Pt NPs with sizes tunable from 3 nm to 7 nm, and controlled polyhedral, truncated cubic, or cubic shapes, and the study of their catalysis for the ORR under PEMFC reaction conditions. A rotating disk electrode (RDE) was used to eliminate O_2 diffusion near the electrode and to analyze intrinsic catalytic ORR activity of the platinum catalysts in 0.5 M H_2SO_4. The current density from the ORR for platinum nanocubes is four times that of polyhedral platinum or the truncated cubic Pt NP catalyst, indicating that the ORR activity is indeed dependent on the shape, not on the size, of the Pt NPs.

In the synthesis (see the Experimental Section), the size and the shape of the Pt NPs were controlled by reaction temperature at which $Fe(CO)_5$ was injected into the $Pt(acac)_2$ solution. For example, injecting $Fe(CO)_5$ at 180 °C gave 3 nm polyhedral platinum, at 160 °C yielded 5 nm truncated cubic platinum, whereas at 120 °C followed by controlled heating at 3–5 °C min^{-1} to 200 °C, 7 nm cubic platinum was produced. Without $Fe(CO)_5$, Pt NPs were still prepared, but both the size and shape of the particles were much less controlled. Figure 1 shows representative transmission electron microscopy (TEM) images of the 3 nm, 5 nm, and 7 nm Pt NPs (more TEM images are given in the Supporting Information, Figure S1 and S2). Selected area electron diffraction of the nanocube assembly (see the Supporting Information, Figure S1a) gives a pattern of bright spots arranged with four-fold symmetry (Supporting Information, Figure S1b), indicating the formation of a (100) texture in the assembly. Quantitative elemental analyses with a scanning electron microscope (SEM) equipped with spatially resolved energy-dispersive X-ray spectroscopy show that iron cannot be detected on the surface of the Pt NPs, indicating that the trace amount of iron added during the synthesis is only involved in the formation of nuclei.

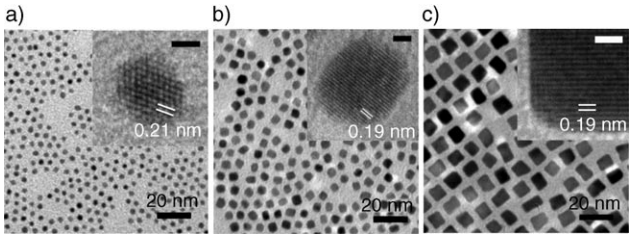

Figure 1. Representative TEM images of a) the 3 nm polyhedral b) the 5 nm truncated cubic and c) the 7 nm cubic Pt NPs. The insets are the representative HRTEM images of corresponding single particles, showing a) Pt(111), b) Pt(100), and c) Pt(100) lattice fringes. All scale bars in the insets correspond to 1 nm.

The crystal structure of the Pt NPs was obtained by X-ray diffraction (XRD). The diffraction patterns from different NPs (Figure 2) indicate that the particles have the face-

[*] C. Wang, T. Koda, Prof. S. Sun
Department of Chemistry
Brown University
Providence, RI 02912 (USA)
Fax: (+1) 401-863-9046
E-mail: ssun@brown.edu
H. Daimon, T. Onodera, T. Koda
Technology & Development Division
Hitachi Maxell Ltd.
6-20-1 Kinunodai, Tsukubamirai, Ibaraki 300-2496 (Japan)

[**] The work was supported by NSF/DMR 0606264, a Brown University Research Seed Fund and a scholarship from Hitachi Maxell, Ltd.

Supporting information for this article is available on the WWW under http://www.angewandte.org or from the author.

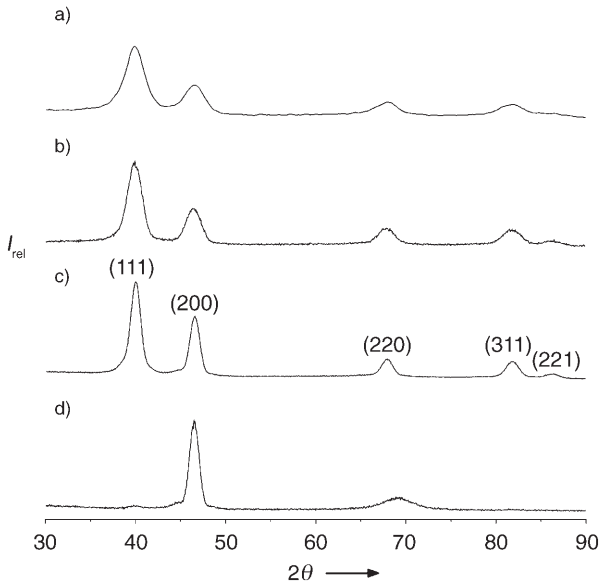

Figure 2. XRD patterns of a) the 3 nm polyhedral, b) the 5 nm truncated cubic, c) the 3D randomly oriented 7 nm cubic and d) the (100) textured 7 nm cubic Pt NP assemblies.

centered cubic (fcc) structure, and the NP sizes estimated from Scherrer's formula are consistent with that measured in the respective TEM images, indicating the presence of single crystals. For the 3 nm and 5 nm Pt NPs, the (111) peak is much stronger than the (200) peak. This is expected for a three-dimensional randomly oriented assembly. For the 7 nm nanocubes, fast evaporation of the NP dispersion led to an almost three-dimensionally randomly oriented assembly (Figure 2c), but slow evaporation of the solvent resulted in a (100) textured assembly, as seen by the dominant (200) peak in Figure 2d. This result confirms that the 7 nm nanocubes are surrounded by {100} planes, and have a very narrow shape distribution.

The synthesis reported herein indicates that the presence of trace $Fe(CO)_5$ facilitates fast platinum nucleation and growth of Pt NPs with controlled size and shape. The formation of platinum nuclei was seen by a color change of the solution to black immediately after the injection of $Fe(CO)_5$ at high temperatures (160 °C and 180 °C). If $Fe(CO)_5$ was injected at 120 °C, the solution was dark yellow, but turned to black when it was heated to 160 °C. The shape of the nuclei is likely to be polyhedral, as it is known that in the growth of fcc-structured nanocrystals, the nuclei formed in the early stage of the synthesis tend to adopt a polyhedral shape to minimize their surface energy.[7,10] In the fast nucleation/growth process at higher injection temperatures, most of the platinum precursors are consumed, and there is no preference for the growth in ⟨100⟩ and ⟨111⟩ directions. As a result, small polyhedral Pt NPs are formed. Injection of $Fe(CO)_5$ at a lower temperature (120 °C) followed by a slow rate of heating facilitates a slow nucleation/growth process, which leads to the thermodynamic growth along the ⟨111⟩ over the ⟨100⟩ direction and the formation of larger cubes.

The growth process can be monitored by quenching the reaction at different temperatures (see the Supporting Information, Figure S3). Pt NPs were obtained by taking aliquots of the reaction solution at 170 °C and 200 °C during the synthesis of 7 nm platinum nanocubes. The particles were precipitated quickly by adding isopropanol to the octadecene solution, and the product was separated by centrifugation and redispersed in hexane. At 170 °C, the size of the particles reached 4–5 nm, but the shape was polyhedral/truncated cubic. At 200 °C, the NPs grew into 7 nm cubes owing to the preferred growth on {111} over {100} facets.

To remove the organic coating around the NPs for ORR studies, the Pt NPs were dispersed in hexane, then separated by adding ethanol followed by centrifugation. The NPs were washed by ethanol a further three times and irradiated by UV light (185 nm and 254 nm) for 24 h in air.[11] SEM images of the 5 nm truncated cubic and 7 nm cubic Pt NPs after the irradiation (see the Supporting Information, Figure S4) show that the treatment does not lead to any obvious NP morphology change.

The Pt NPs were prepared for electrochemical measurements (see the Experimental Section). CVs were measured at 308 K with potential scanned from 0.03 V to 0.5 V versus the normal hydrogen electrode, NHE, as shown in Figure 3. The

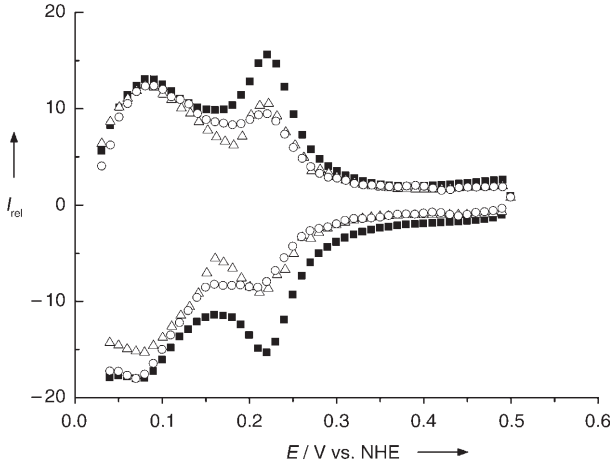

Figure 3. CVs of the Pt NPs (○ polyhedron, △ truncated cube, ■ cube). The potential was applied with a scanning rate of 10 $mV s^{-1}$.

peak at about 0.22 V originates from the hydrogen adsorption/desorption on the Pt(100) face, and the increased peak intensity reflects the fact that more (100) planes are present on the NP surface.[5] This result also shows that the surfactants have been successfully removed by the UV treatment; without this treatment, only featureless CV curves were obtained. It can be seen from Figure 3 that the 7 nm nanocubes have more (100) planes exposed to the solution. This is consistent with the TEM and XRD analyses, for which it was found that the surface of the nanocubes is dominated by (100) facets.

The catalytic activity of the Pt NPs for the ORR was measured with an RDE (see the Experimental Section). The current densities (J, $mA cm^{-2}$) were calculated by dividing the measured electrode currents with the surface areas obtained from the hydrogen desorption in Figure 3. Figure 4a shows

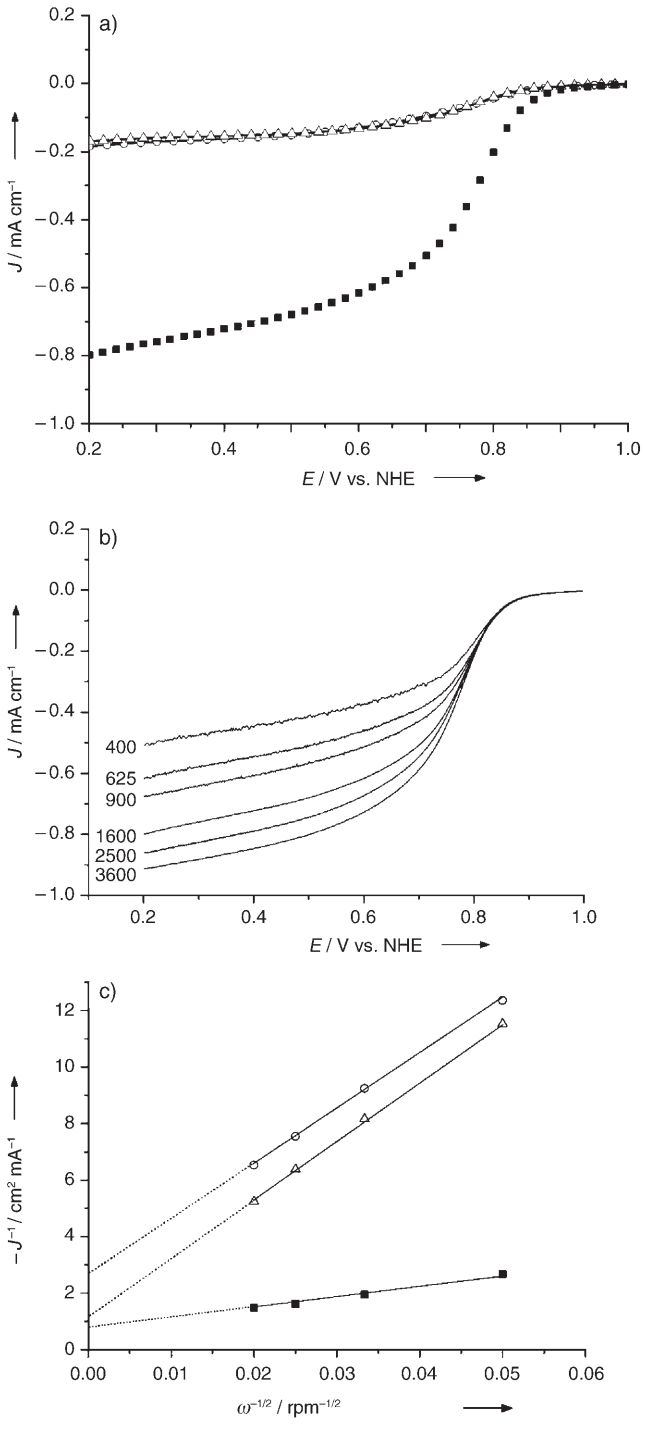

Figure 4. a) Disk current densities in oxygen saturated 0.5 M H_2SO_4 as a function of potential the platinum catalysts (○ polyhedron, △ truncated cube, ■ cube) at a rotation speed of 1600 rpm. b) Rotation-rate-dependent current–potential curves for 7 nm platinum nanocubes. c) Koutecky–Levich plots at 0.6 V for the platinum catalysts (△ polyhedron, ○ truncated cube, ■ cube). The potential was applied with scanning rate of 10 mV s^{-1}.

the electrode current densities of the ORR for the Pt NPs. The overpotential for the ORR is reduced by nearly 50 mV by the 7 nm platinum nanocubes compared with the other Pt NPs, and can be seen from the onset ORR potentials at ca. 0.92 V for the 7 nm Pt NPs and ca. 0.87 V for the 3 nm and 5 nm Pt NPs. Around the half-wave potential (ca. 0.75 V), the current density generated from the 7 nm Pt NPs is about four times that of either 3 nm or 5 nm NPs. This catalytic enhancement in the ORR for the Pt(100)-dominated nanocubes is consistent with what have been observed in Pt(hkl)-dependent ORR activities from the extended electrode surfaces.[5]

The NP shape-dependent ORR activity can be ascribed to different adsorptions of sulfate ions on Pt (111) and (100) facets. Sulfate ions tend to bind to the platinum surface atoms in solution and impede the ORR activity. The trend of binding strength is (111) ⩾ (100) owing to the matching threefold symmetry between three equivalent oxygen atoms in the sulfate and platinum atoms on the (111) layer (see the Supporting Information, Figure S5).[13] For the ORR, the case is reversed, and the (100) facet has more active sites than (111) in H_2SO_4. The nanocubes have dominant (100) facets, and therefore the high ORR activity. The similar low reactivity observed from both 3 nm and 5 nm NPs is consistent with a recent report on size independence of the Pt NPs on fuel-cell activity.[9] The shape-dependent catalysis further proves that a trace amount of iron in the Pt NPs does not contribute to the activity increase in the NP catalyst.

Rotation-rate-dependent current density–potential curves of the 7 nm platinum nanocubes are given in Figure 4 b (similar curves from the 3 nm and 5 nm Pt NPs are given in the Supporting Information, Figure S6). High rotational speeds result in the increase in oxygen diffusion to electrode surface and large currents. The measured disk electrode current density (J) at different constant potentials can be applied into Levich–Koutecky plots [Equation (1)]:[14]

$$\frac{1}{J} = \frac{1}{J_K} + \frac{1}{J_{\text{diff}}} = \frac{1}{J_K} + \frac{1}{B\,\omega^{1/2}}, \qquad (1)$$

in which

$$B = \frac{0.62\,n\,F\,C_0\,D_0^{2/3}}{\eta^{1/6}}$$

where J_k is the kinetic current density and J_{diff} the diffusion-limiting current density, n is the overall number of electrons transferred, F is the Faraday constant, C_0 is the O_2 concentration in the electrolyte (1.26×10^{-3} mol L^{-1}), D_0 is the diffusion coeficient of O_2 in the H_2SO_4 electrolyte (1.93×10^{-5} cm^2 s), and η is the viscosity of the electrolyte (1.009×10^{-2} cm^2 s).[5] In the J^{-1} versus $\omega^{-1/2}$ plot, the slope is $1/B$. The so-called B factor can be applied to obtain the number of electrons involved in the ORR. Figure 4 c shows the J^{-1} versus $\omega^{-1/2}$ plots at 0.6 V for different platinum catalysts. The number of electrons calculated from the slop is 3.6 for the 7 nm platinum nanocubes, and 0.7 for the 3 nm and 5 nm Pt NPs. This indicates that there is a nearly complete reduction of O_2 to H_2O, a four-electron process, on the cubic surface of the 7 nm platinum. However, the ORR is much less efficient on the 3 nm and 5 nm Pt NP surfaces, which is very likely due to strong sulfate adsorption on their (111) facets.

We have demonstrated a general synthetic approach to monodisperse Pt NPs with controlled sizes (3–7 nm) and shapes (polyhedron, truncated cube and cube) by reaction of $Pt(acac)_2$ with oleic acid and oleylamine in the presence of trace amount of $Fe(CO)_5$. The Pt NPs deposited on glassy carbon electrodes are active catalysts for the ORR in H_2SO_4 medium. The current density measured from the RDE for 7 nm platinum nanocubes is four times that of 3 nm polyhedral (or 5 nm truncated cubic) Pt NPs, indicating a dominant effect of NP shape on the ORR in PEMFC reaction conditions. Work in preparing a highly efficient platinum nanocube catalyst for applications in PEMFCs is underway.

Experimental Section

Typical synthesis of 3 nm polyhedral NPs: $Pt(acac)_2$ (0.1 g), octadecene (10 mL), oleic acid (OA) (1 mL), and oleylamine (OAm) (1 mL) were mixed under N_2 and magnetic stirring. The mixture was then heated to ca. 65 °C to dissolve $Pt(acac)_2$. The temperature was then raised to about 180 °C. A solution of $Fe(CO)_5$ in hexane (0.1 mL, prepared by adding 0.1 mL $Fe(CO)_5$ in 1 mL hexane under argon) was quickly injected into the hot solution. The solution was further heated to 200 °C and kept at this temperature for 1 hour before it was cooled down to room temperature. 40 mL of isopropanol was added and then the suspension was centrifuged (8000 rpm, ca. 10 min) to separate the NPs. The particles were dispersed in ca. 10 mL hexane and precipitated out by adding ethanol. The process was repeated one more time to purify the NPs. The final product (ca. 50 mg) was dispersed in 10 mL of hexane for further use.

5 nm truncated-cubic and 7 nm cubic Pt NPs were synthesized by similar procedures to that described for the synthesis of 3 nm Pt NPs except that $Fe(CO)_5$ was injected at 160 °C and 120 °C, respectively.

Characterization: Samples for TEM analysis were prepared by depositing one drop of diluted NP dispersion in hexane on amorphous carbon-coated copper grids. Images were obtained by a Philips EM 420 (120 kV). High-resolution TEM images were obtained on a JEOL 2010 TEM instrument (200 kV). XRD patterns were obtained on a Bruker AXS D8-Advanced diffractometer with $Cu_{K\alpha}$ radiation ($\lambda = 1.5418$ Å). SEM images were obtained on a Hitachi S-5200 scanning electron microscope. Quantitative elemental analyses were carried out on a LEO 1560 SEM equipped with spatially resolved energy-dispersive X-ray spectroscopy (EDS). Samples for EDS were prepared by depositing the NP dispersion on a silicon substrate and solvent was allowed to evaporate under ambient conditions.

Electrochemical measurements were performed on an electrochemical analyzer, model HR-201 from Hokuto Denko Corp. The treated NPs were dispersed in water by vigorous stirring and sonication. The concentration of NPs was adjusted to 2 mg mL^{-1}, and 20 μL of the solution was dropped onto a glassy carbon electrode (GCE; 5 mm in diameter from Hokuto Denko Corp., Japan). After water evaporation under a partial vacuum for 30 h, 10 μL of 0.1 wt% Nafion solution was dropped on the electrode surface to cover and stabilize the NP assembly on the electrode surface. The platinum-loaded GCE was immersed into 0.5 M H_2SO_4 as a working electrode. The electrochemically active surface area of the Pt NP catalyst was determined by hydrogen desorption in the cyclic voltammogram (CV).[12] Platinum wire was used as a counter electrode, and Ag/AgCl as the reference electrode. 0.5 M H_2SO_4 was chosen as electrolyte over $HClO_4$ or H_3PO_4 owing to its stability and the superior performance in proton transport through the Nafion membrane in PEMFCs.[2] CVs were measured with nitrogen purging at 308 K, with the potential scanned from 0.03 V to 0.5 V versus NHE, and the CVs were used to calculate the surface area of the catalysts. ORR activities were measured under oxygen purging in O_2-saturated 0.5 M H_2SO_4 at 308 K with an RDE (rotation speed 400–4500 rpm).

Received: January 7, 2008
Revised: March 4, 2008
Published online: April 9, 2008

Keywords: fuel cells · heterogeneous catalysis · nanoparticles · oxygen · platinum

[1] a) K. Temple, F. Jäkle, J. B. Sheridan, I. Manners, *J. Am. Chem. Soc.* **2001**, *123*, 1355; b) T. Shimada, I. Nakamura, Y. Yamamoto, *J. Am. Chem. Soc.* **2004**, *126*, 10546; c) K. Godula, D. Sames, *Science* **2006**, *312*, 67; d) K. M. Bratlie, H. Lee, K. Komvopoulos, P. Yang, G. A. Somorjai, *Nano Lett.* **2007**, *7*, 3097.
[2] N. P. Brandon, S. Skinner, B. C. H. Steele, *Annu. Rev. Mater. Res.* **2003**, *33*, 183.
[3] N. M. Markovic, P. N. Ross, *Surf. Sci. Rep.* **2002**, *45*, 117.
[4] a) T. Toda, H. Igarashi, H. Uchida, M. Watanabe, *J. Electrochem. Soc.* **1999**, *146*, 3750; b) V. R. Stamenkovic, B. S. Mun, M. Arenz, K. Mayrhofer, C. A. Lucas, G. Wang, P. N. Ross, N. M. Markovic, *Nat. Mater.* **2007**, *6*, 241; c) H. Yano, M. Kataoka, H. Yamashita, H. Uchida, M. Watanabe, *Langmuir* **2007**, *23*, 6438.
[5] N. M. Markovic, H. A. Gasteiger, P. N. Ross, *J. Phys. Chem.* **1995**, *99*, 3411.
[6] a) T. S. Ahmadi, Z. L. Wang, T. C. Green, A. Henglein, M. A. EI-Sayed, *Science* **1996**, *272*, 1924; b) M. Yamada, S. Kon, M. Miyake, *Chem. Lett.* **2005**, *34*, 1050; c) T. Herricks, J. Chen, Y. Xia, *Nano Lett.* **2004**, *4*, 2367; d) J. Chen, T. Herricks, Y. Xia, *Angew. Chem.* **2005**, *117*, 2645; *Angew. Chem. Int. Ed.* **2005**, *44*, 2589; e) H. Lee, S. E. Habas, S. Kweskin, D. Butcher, G. A. Somorjai, P. Yang, *Angew. Chem.* **2006**, *118*, 7988; *Angew. Chem. Int. Ed.* **2006**, *45*, 7824; f) J. Solla-Gullón, V. Montiel, A. Aldaz, J. Clavilier, *J. Electroanal. Chem.* **2000**, *491*, 69; g) X. Teng, H. Yang, *Nano Lett.* **2005**, *5*, 885; h) B. Mayers, X. Jiang, D. Sunderland, B. Cattle, Y. Xia, *J. Am. Chem. Soc.* **2003**, *125*, 13364; i) J. Chen, Y. Xiong, Y. Yin, Y. Xia, *Small* **2006**, *2*, 1340.
[7] J. Ren, R. D. Tilley, *J. Am. Chem. Soc.* **2007**, *129*, 3287.
[8] C. Wang, H. Daimon, Y. Lee, J. Kim, S. Sun, *J. Am. Chem. Soc.* **2007**, *129*, 6974.
[9] a) H. Yano, J. Inukai, H. Uchida, M. Watanabe, P. K. Babu, T. Kobayashi, J. H. Chung, E. Oldfield, A. Wieckowski, *Phys. Chem. Chem. Phys.* **2006**, *8*, 4932; b) H. Yano, E. Higuchi, H. Uchida, M. Watanabe, *J. Phys. Chem. B* **2006**, *110*, 16544.
[10] W. Romanowski, *Surf. Sci.* **1969**, *18*, 373.
[11] W. Chen, J. Kim, S. Sun, S. Chen, *Phys. Chem. Chem. Phys.* **2006**, *8*, 2779.
[12] M. Watanabe, M. Tomikawa, S. Motoo, *J. Electroanal. Chem.* **1985**, *182*, 193.
[13] M. E. Gamboa-Aldeco, E. Herrero, P. S. Zelenay, A. Wieckowski, *J. Electroanal. Chem.* **1993**, *348*, 451.
[14] A. J. Bard, L. R. Faulkner, *Electrochemical Methods: Fundamentals and Applications*, Wiley, New York, **2000**.

